

REPORT DOCUMENTATION PAGE

Form Approved
OMB No. 0704-0188

Public reporting for this collection of information is estimated to average 1 hour per response, including the time for reviewing instructions, searching existing data sources, gathering and maintaining the data needed, and completing and reviewing the collection of information. Send comments regarding this burden estimate or any other aspect of this collection of information, including suggestions for reducing this burden, to Washington Headquarters Services, Directorate for Information Operations and Reports, 1215 Jefferson Davis Highway, Suite 1204, Arlington, VA 22202-4302, and to the Office of Management and Budget, Paperwork Reduction Project (0704-0188), Washington, DC 20503.

1. AGENCY USE ONLY (Leave Blank)		2. REPORT DATE 7 May 1992	3. REPORT TYPE AND DATES COVERED Final, 28 Sep 90 - 28 Feb 92	
4. TITLE AND SUBTITLE Ionized Cluster Beams for Space Propulsion <i>LU</i>			5. FUNDING NUMBERS F49620-90-C-0085 <i>23081AS</i>	
6. AUTHOR(S) W.S. Williamson, W. Knauer				
7. PERFORMING ORGANIZATION NAME(S) AND ADDRESS(ES) Hughes Research Laboratories 3011 Malibu Canyon Road Malibu, California 90265			8. PERFORMING ORGANIZATION REPORT NUMBER	
9. SPONSORING/MONITORING AGENCY NAME(S) AND ADDRESS(ES) Air Force Office of Scientific Research Building 410 Bolling AFB, DC 20332-6448 <i>NAF</i>			10. SPONSORING/MONITORING AGENCY REPORT NUMBER	
11. SUPPLEMENTARY NOTES				
12a. DISTRIBUTION/AVAILABILITY STATEMENT			12b. DISTRIBUTION CODE	
13. ABSTRACT (maximum 200 words) Ionized clusters formed from atomic or molecular gases possess higher mass than the heavy inert-gas ions presently used as propellants in electrostatic ion-propulsion systems; this study has investigated the possibility of using these heavy clusters in an electrostatic thruster to permit operation in the intermediate range of specific impulse (1000 to 2000 s) in which there is a need for efficient electric propulsion. Clusters are formed when gases expand through a supersonic nozzle; when a low-mass carrier gas such as hydrogen or helium is added, a large fraction of the heavier thrust gas emerges in the form of clusters. In our experiments, over 90% of carbon dioxide (mixed with hydrogen) formed clusters with typically 250 constituent molecules. These clusters can be ionized with comparably high efficiency and then accelerated electrostatically to provide thrust. Our experiments showed that additional study is needed in several areas, the most critical of which is to find means to reduce the amount of carrier gas required.				
14. SUBJECT TERMS clusters, charged-particle beams, ion propulsion, supersonic nozzle			15. NUMBER OF PAGES 30	
			16. PRICE CODE	
17. SECURITY CLASSIFICATION OF REPORT UNCLASSIFIED	18. SECURITY CLASSIFICATION OF THIS PAGE UNCLASSIFIED	19. SECURITY CLASSIFICATION OF ABSTRACT UNCLASSIFIED	20. LIMITATION OF ABSTRACT	

Accession For	
NTIS GRA&I	<input checked="" type="checkbox"/>
DTIC TAB	<input type="checkbox"/>
Unannounced	<input type="checkbox"/>
Justification	
By _____	
Distribution/	
Availability Codes	
Dist	Avail and/or Special
A-1	



CONTENTS

ILLUSTRATIONS AND TABLES	II
1.0 INTRODUCTION	1
2.0 BASIC CLUSTER-BEAM PHYSICS	4
2.1 Cluster Formation	4
2.2 Cluster Ionization	6
2.3 Cluster-Beam Extraction System	8
2.3.1 Extraction-System Sputtering by Cluster Ions	9
2.3.2 Relationship Between Cluster Mass and Beam Voltage	11
2.3.3 Effects of Cluster/Carrier-Gas Collisions	12
3.1 Test Configuration	14
3.1.1 Pulsed Valve	14
3.1.2 Supersonic Nozzle	15
3.1.3 Ionizer	15
3.1.4 Beam-Extraction System	15
3.1.5 Retarding-Potential Analyzer (RPA)	15
3.2 Test Procedure	15
3.2.1 Thruster Parameters	16
3.2.2 Measurement Methodology	17
3.3 Experimental Results	18
3.4 Supporting Measurements	22
3.2.1 Nozzle Characteristics	22
3.2.2 Ionizer Characteristics	24
3.2.3 Beam Extraction System Characteristics	25
4.0 SUMMARY AND CONCLUSIONS	29
5.0 REFERENCES	31
APPENDIX 1. SYMBOLS USED IN THIS REPORT	32
APPENDIX 2. EFFECT OF MASS-TO-CHARGE DISTRIBUTION ON THRUSTER PERFORMANCE	34

ILLUSTRATIONS AND TABLES

Figure 1. Schematic of the ionized-cluster apparatus used for this study.	3
Figure 2. Pressure and temperature distributions in gas flow.	5
Figure 3. Pressure-temperature diagram of gas expansion.	6
Figure 4. Kinetic energies of atoms or molecules in clusters.	11
Figure 5. Cluster-beam voltage as a function of cluster mass.	12
Figure 6. Clustering efficiencies.	19
Figure 7. Clustering efficiencies measured with gas mixtures.	20
Figure 8. Dependence of clustering efficiencies on the total (stagnation) pressure.	21
Figure 9. Exhaust velocities of single gases (top) and of a gas mixture (bottom).	23
Figure 10. Calculated and measured nozzle flow rates.	24
Figure 11. Cluster size and current as a function of ionizer current.	25
Figure 12. Retarding potential characteristic of the cluster current	26
Figure 13. Comparison between plasma and cold cathode ionizers.	27
Figure 14. Observation of space-charge-limited flow.	28
Figure 15. Transverse cluster beam distribution.	28
Table 1. Ionized-Cluster Thruster Performance.	22

1.0 INTRODUCTION

While a wide variety of propulsion systems have been developed over the years, a gap has developed in the medium range of specific impulse (roughly 1000 to 2000 s) for which no advanced electric-propulsion system is ready. Chemical rockets cover the territory below 300 s effectively, and state-of-the-art ion thrusters are highly efficient in the ≥ 3000 -s regime.

The concept of the orbit-transfer vehicle (OTV) has evolved in recent times; these vehicles, which would carry spacecraft from low orbits to higher orbits, would be optimally served by a propulsion system with a specific impulse I_{sp} in the 1600-s range. (Appendix 1 lists all symbols used in this report.) The OTV performance requirement that drives this optimum is the need to achieve short trip times with the available onboard electrical power; that is, the ratio thrust/power F/P is determined by the available power P and the thrust F needed to achieve the desired trip time. This ratio of thrust to power must be provided with minimum propulsion-system mass, to avoid degrading the payload-mass/spacecraft-mass ratio. The two key relationships are

$$F / P = \frac{2\eta_T}{gI_{sp}} \quad (1.0-1)$$

and

$$I_T = M_p g I_{sp}, \quad (1.0-2)$$

where η_T is the total efficiency of the thrust system, g is the acceleration due to gravity, I_T is the total mission impulse requirement (total thrust x time), and M_p is the total propellant mass. These relationships show the importance of specific impulse in determining propellant mass and specific impulse combined with overall thruster efficiency in determining thrust-to-power ratio. The equations show the conflicting trends toward high specific impulse to minimize propellant mass and low specific impulse to maximize thrust-to-power ratio and therefore to minimize trip time.

Equations 1.01-1 and 1.01-2 can be combined to find

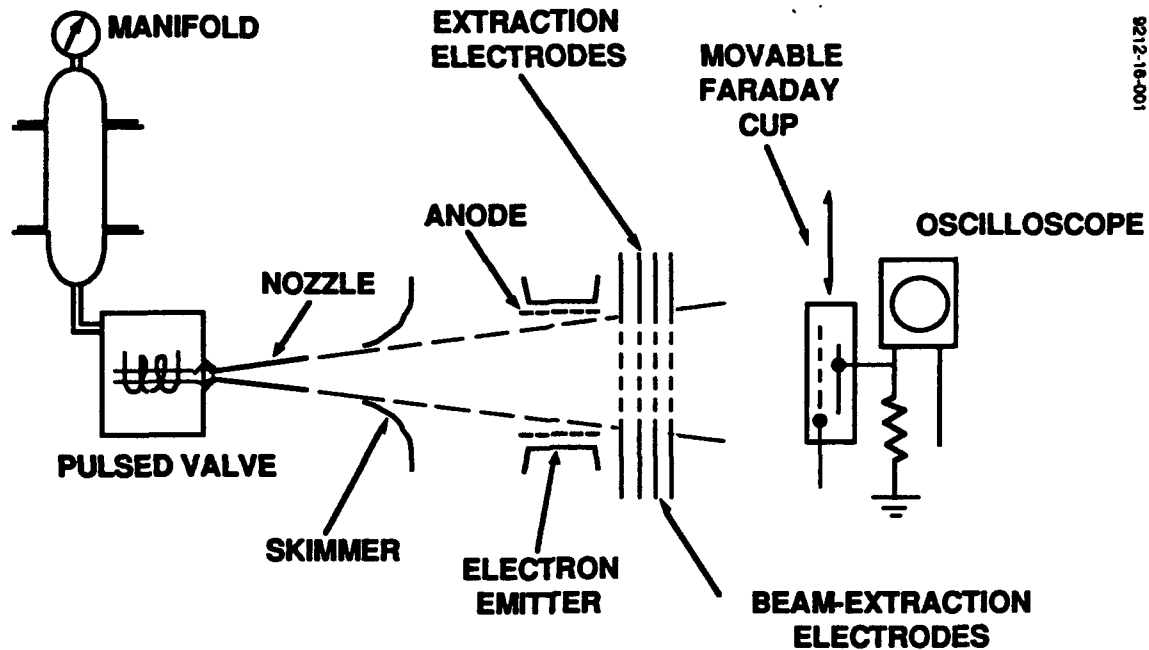
$$M_p = \frac{I_T}{2\eta_T} \left(\frac{F}{P} \right); \quad (1.0-3)$$

that is, for a given thrust-to-power requirement, the total propellant mass is inversely proportional to the total thrust-system efficiency, η_T ; if the total efficiency is 50%, then twice the propellant mass is needed, compared to an ideal thruster.

Several novel thrust systems have been developed in response to the OTV requirement for medium specific impulse. Rocket Research Company, for example, has developed a flightready arcjet thruster that will be flown on the GE Astrospace Series 7000 satellite, beginning in 1993. The 6-kg-mass thruster operates on a power of 1.8 kW to produce thrust at specific impulse of ≥ 500 s. A similar but larger, 26-kW ammonia arcjet operates at a specific impulse of 812 s, and is expected to be flight tested in 1995. The former Soviet Union had developed a "stationary-plasma" thruster operating at 1600 s of specific impulse, providing up to 350 mN of thrust at a 6-kW power level. Still, these devices have certainly not closed the specific-impulse gap: the arcjets still operate at an undesirably low level of specific impulse, and the Russian device appears to experience severe life-limiting erosion processes.

Conventional ion thrusters, employing inert-gas propellants such as xenon, can operate at low specific impulse simply by using reduced beam voltages. However, two problems arise which have thus far prevented the development of capable thrusters in the 1000-to-2000-s specific-impulse range: first, the thruster electrical efficiency η_E falls off with low extraction voltages; and second, operation at low beam voltage requires high beam currents to provide unreduced thrust, but the high beam currents cause early wearout of the extraction grids. If a heavy propellant particle were available, thrust could be provided at higher beam voltages and lower beam currents, and these problems would be averted. Clusters, with their high mass compared to monoatomic inert gases, offer the promise of filling this need.

Figure 1 shows our concept for ion propulsion using ionized clusters. The basic idea is that atomic or molecular species introduced into the nozzle shown on the left will, under conditions discussed in the next section, condense into clusters ranging from a few hundred to a few thousand atoms. These clusters can be readily ionized and accelerated to high energy, just as if they were heavy monoatomic inert gases.



9212-16-001

Figure 1. Schematic of the ionized-cluster apparatus used for this study.

Under this contract, we have made use of an apparatus constructed under a previous effort¹ to test the idea of using clusters to form a heavy propellant ion for space-propulsion applications. Basically, we have been successful in this attempt, although a great deal of additional work remains to be done to bring the concept to application. We have been able to demonstrate thrust levels above 10 mN in our relatively primitive laboratory apparatus, and we have achieved near-complete clusterization of carbon-dioxide gas, when supplied with hydrogen carrier gas to aid in the cluster-condensation process. Our work builds upon earlier studies² in achieving high clusterization with molecular gases; molecular gases form smaller clusters with masses around 15,000 amu, compared to inert-gas clusters, which typically have masses of the order of 250,000 amu. The smaller-mass clusters allow beam formation with lower voltages, which may be a practical advantage.

The key processes that appear to block the path of ionized-cluster beams as a means of space propulsion are the need for excessive amounts of carrier gas (which degrades the propellant-utilization efficiency), the poor performance of the ionizer (which requires excessive power and produces excessively wide distributions of mass-to-charge ratio) and the beam-extraction system, which accelerates only a small fraction of the incident ionized-cluster current. We believe that all of these difficulties may yield to further investigation, and the preliminary accomplishments that we have made in this study may lead to a viable space-propulsion system.

2.0 BASIC CLUSTER-BEAM PHYSICS

In this section we describe the basic processes by which ionized cluster beams are formed: cluster nucleation and growth with supersonic nozzles and carrier gases, cluster ionization with electron bombardment, and the extraction and formation of an ionized-cluster beam. We will also discuss the characteristics of ion-propulsion systems so that we can evaluate the potential of ionized cluster beams for space-propulsion applications.

2.1 CLUSTER FORMATION

In this section we present a simple model which illustrates the principal elements of the phenomena that are observed in gas expansion through supersonic nozzles under a specific set of conditions. This model is similar to others^{3,4} that have appeared previously in the literature.

Clusters are formed when gas expanding through a supersonic nozzle cools to the supersaturation point; it then begins to nucleate and condense, forming clusters. Figure 2 illustrates the basic geometry for cluster formation in a supersonic nozzle. Gas is supplied to the nozzle at the *stagnation pressure*, which is the pressure corresponding to the nonflowing gas within the supply reservoir. If the gas expands without heat addition or frictional losses (i.e., the expansion is *isentropic*), then the internal energy and pressure of the gas is converted into kinetic motion of the atoms or molecules. During this isentropic expansion the temperature of the gas decreases, following the curve shown in Fig. 3. For ideal gases, the isentrope can be characterized by the equation

$$TV^{\gamma-1} = \text{const.} , \quad (2.1-1)$$

where $\gamma = c_p/c_v$, and c_p and c_v are the specific heats of the gas at constant pressure and volume, respectively. When the pressure and temperature of the expanding gas pass to the left of the vapor-pressure curve (refer to Fig. 3) for the particular gas in question, it enters a region of supersaturation, i.e., the vapor density is above that which can be sustained at the given temperature. In this transient condition, the gas will begin to condense, forming nuclei which eventually grow into clusters. During condensation, however, the latent heat of condensation is released, which briefly increases the temperature and pressure of the expanding gas as illustrated in Fig. 2. This increase in temperature brings the gas back to

the vapor-pressure curve, and acts as feedback mechanism, preventing further excursions into the supersaturation region.

According to Reference (3), cluster nuclei are formed during the brief initial excursion into the supersaturation region. These clusters will continue to grow as long as the collision frequency with unclusterized atoms or molecules is significant, but additional clusters are not formed.

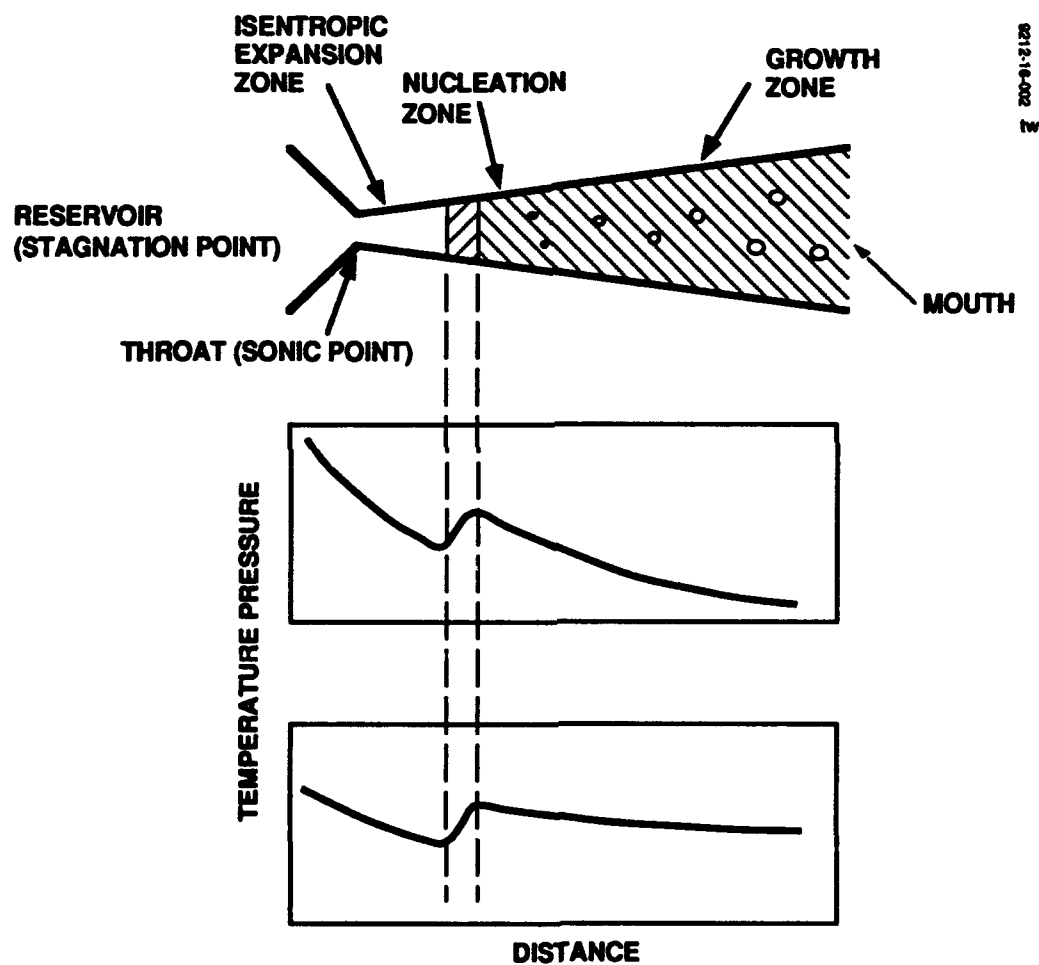


Figure 2. Pressure and temperature distributions in gas flow through a supersonic nozzle with condensation. According to Oswatitsch³ nucleation takes place only within a narrow zone, while cluster growth continues along much of the nozzle.

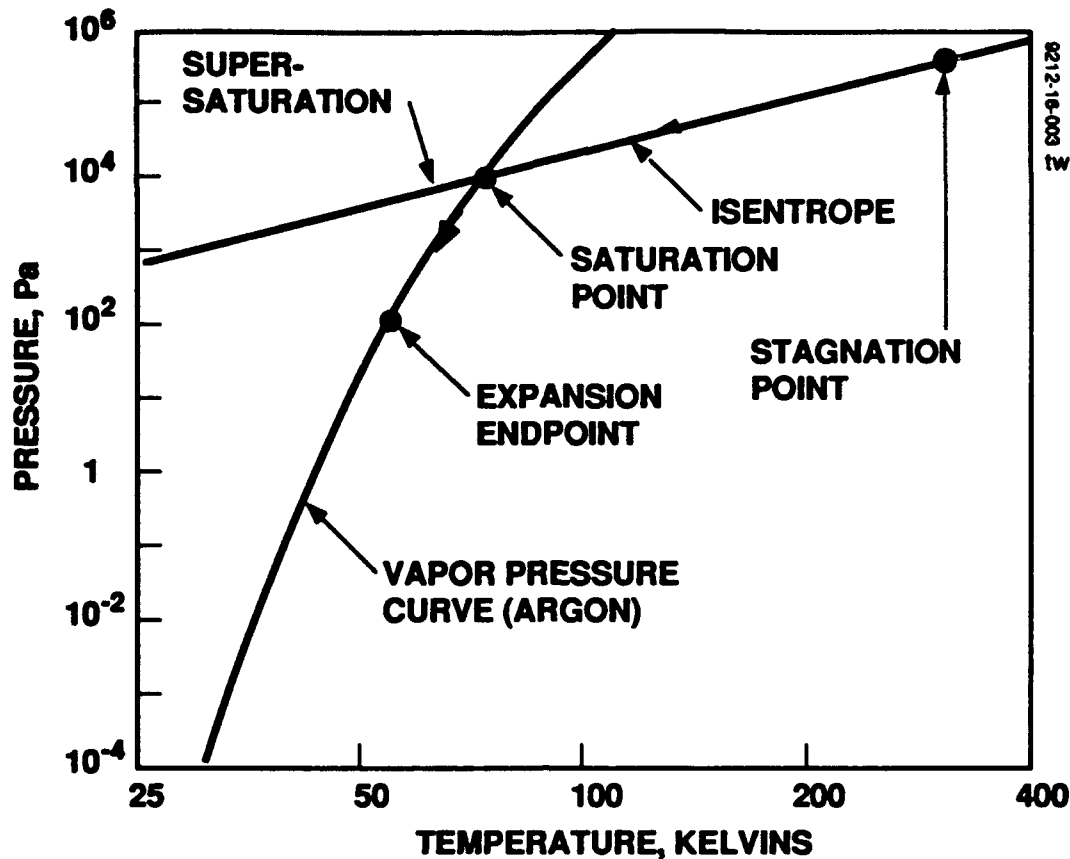


Figure 3. Pressure-temperature diagram of gas expansion in a supersonic nozzle with condensation. As the gas enters the nozzle it expands isentropically at first. When it reaches the point of saturation, condensation can set in. On its further expansion, the gas tracks the vapor pressure curve and absorbs the latent heat of condensation as it proceeds.

2.2 CLUSTER IONIZATION

Cluster ionization is obtained in our experimental apparatus by neutral-cluster bombardment with electrons derived from a ring-shaped filament and accelerated through a cylindrical screen-mesh anode.

The electron current in the ionizer required to assure near-complete ionization of the neutral cluster beam can be estimated from a simple collision-cross-section calculation:

$$j_e = \frac{v_{cl}}{L} \frac{1}{\sigma_i N}, \quad (2.2-1)$$

where $N = 300$ to 600 is the number of atoms in a cluster, $v_{cl} = 10^3$ m/s is the cluster velocity, $\sigma_i = 2$ to 3×10^{-20} m² are typical ionization cross sections, and using an ionizer axial length of $L = 20$ mm, we find that current densities of the order of $j_e = 1$ kA/m² (100 mA/cm²) are needed to ensure a high ionization fraction. (Experimentally, we have found that increasing the electron current density causes the cluster-beam current to increase

until electron current densities near the 1 kA/m² value are reached; this observation seems to confirm our rough calculation.)

In order to extract the magnitude of electron current just determined, we must design an ionizer within the constraints of the Child-Langmuir space-charge limit on current density:

$$j_e = \frac{4\epsilon_0}{9z_0^2} \sqrt{\frac{e}{m_e}} V_D^{3/2}, \quad (2.2-2)$$

where z_0 is the cathode-to-anode gap, ϵ_0 is the permeability of free space, V_D is the electron accelerating voltage (discharge voltage), and e and m_e are the charge and mass of the electron, respectively. Using a typical value of $V_D = 100$ V, we find that we require a gap $z_0 \leq 1.6 \mu\text{m}$ in order to achieve the required 1 kA/m². Maintaining such a small gap between two material electrodes is obviously impractical (particularly when one—the filament—must be heated to roughly a 2000-K temperature). However, the presence of ionized atomic species (ions formed from unclustered thrust gas and carrier gas atoms) leads to the formation of a plasma sheath between the anode and cathode which greatly narrows the effective anode-cathode gap below the physical separation of the metal electrodes.

As is well known in plasma diodes similar to our ionizer, the bulk of the plasma remains near anode potential, and the 100-V discharge voltage appears across a thin sheath near the cathode. The characteristic thickness of the sheath is the plasma Debye length, which is in the 40- μm range in plasmas of modest density ($n_e \approx 10^{17} \text{ m}^{-3}$). We believe that the presence of this ionizer-filling plasma, formed of the waste (non-cluster) gases emanating from the supersonic nozzle, serves two important functions: it permits extraction of high electron-current densities, as just described, and it also causes nearly all of the clusters to become ionized at the same electrostatic potential—that of the anode plasma.

The foregoing observations point to the need for further work in two specific areas: improved ionizer design to exploit plasma effects, and adjustment of the electron energy eV_D to provide as uniform as possible a mass-to-charge ratio, M_C/q . In the case of ionizer design, we feel that incorporating modern magnetic-confinement methods (which have been highly developed in Penning-discharge ion thrusters) could dramatically improve ionizer efficiency in terms of the ionizer power required to ionize an ampere of cluster-beam current. In the case of the mass-to-charge ratio, we will show in a later section that having a broad spread in M_C/q significantly degrades the efficiency of any cluster-beam thruster that could be designed. While some spread in M_C/q is inevitable due to the randomness of the clusterization process, the fact that the ionizer creates cluster ions with charges ranging from $q = e$ to $4e$ imposes an unacceptable loss in thrusting efficiency. While we have not yet attempted to reduce the range of cluster charges, we feel that a narrower distribution could be achieved by combining reduced electron energy (around 40 eV) with the greater ionizer control and efficiency afforded by the Penning discharge.

2.3 CLUSTER-BEAM EXTRACTION SYSTEM

The cluster-beam extraction system that we have employed is a derivative of electrostatic beam-forming technology that has been developed for application in ion thrusters and broad-beam industrial ion sources over the last 30 years, with a simple modification to exclude efficiency-degrading light ions from the beam. We want our extraction system to form its beam without extracting light ions and to accelerate heavier ions without significant interception of ion trajectories by the grids themselves. When there is interception, we require that the energy per incident ion be below the sputter threshold⁵ so that the grids will not be rapidly eroded away.

A common embodiment of the broad-beam extraction system employs three grids, each fabricated from a thin refractory metal (commonly, molybdenum) with a densely packed hexagonal pattern of apertures. The apertures between the three grids are aligned in such a manner that the emerging beamlets are parallel to the thrust axis. In the case of flat grids, the apertures are paraxial; if the grids are formed into spherical caps for mechanical stability (as is common practice), then the apertures must be slightly displaced or *compensated* to provide paraxial beamlets and avoid cosine-law thrust loss. The three grids are biased as follows: the innermost or *screen* grid is maintained at the high positive beam voltage, the intermediate or *accel* grid is held negative (typically a few hundred volts) to prevent electrons from outside the thruster from flowing upstream into the thruster, and the outermost or *decel* grid is at ground potential.

Ion trajectories in a three-grid beam extraction system vary primarily because of differences in the point of entry into the beam-extraction system and because of ion-temperature effects. In our cluster beams, however, the mass-to-charge ratio varies widely, due to the formation of multiply charged clusters and to the statistical variation in cluster masses formed in the supersonic nozzle. This mass variation, which has been observed to be gaussian in character,⁴ will potentially lower the thrust density because the species having higher mass-to-charge ratio will cause the extraction to become perveance limited prematurely. Another potentially troubling problem is that many carrier-gas atoms become ionized; their masses of 2 to 4 amu compare with 20 to 50 x 10³ amu for molecular and inert-gas clusters. These light ions pose a twofold problem: they seriously degrade thruster performance, as noted above, and they can cause extraction-system design to become difficult because of the very different initial velocities of the cluster ions and the light ions. Fortunately, we have a simple solution to the light-ion problem: our ion-extraction system incorporates a fourth grid inside the screen grid to reject light ions. If the potential on the retarding grid is V_R , then clusters having a mass-to-charge ratio of

$$\frac{M_d}{q} = \frac{2eV_R}{v_d^2} \quad (2.3-1)$$

or more will be accepted into the extraction system; lighter ions or clusters will be rejected. The comparatively small fraction of these lighter ions makes the mass-utilization cost of this approach a small one.

2.3.1 Extraction-System Sputtering by Cluster Ions

The remaining beam-extraction issue confronting a practical ionized-cluster thruster is sputtering of extraction grids by clusters themselves. First of all, there are three types of sputtering to consider, corresponding to the specific grid involved :

- Type 1. Screen-Grid Sputtering by impact of those clusters that strike the upstream side of the screen grid,
- Type 2. Charge-Exchange Sputtering of the accel grid by ions that are formed when ionized clusters strike neutral gas atoms (carrier gas or unclusterized thrust gas) and transfer some charge to the neutral, and
- Type 3. Direct Interception of ionized clusters that strike grids after they have been accelerated to high energy.

Sputtering of the fourth (retarding) grid is unlikely to occur, since it is biased positive with respect to anode voltage, and the decel is unlikely to be sputtered by charge-exchange ions because of their low energy. We discuss these three types separately below.

Type-1 sputtering is trivially limited by keeping the energy of the incident ionized clusters below the sputter threshold of the screen grid. Since most of this energy is acquired through acceleration from the ionizer-plasma potential to the screen, it is trivially controlled by maintaining ionizer plasma potentials low. In our experiments, we have no ability to investigate this approach, since our ionizer does not employ any form of magnetic confinement and achieves efficient ionization only when the voltages are near 100 V.

Type-2 sputtering normally results from the fact that the accel grid must be held negative several hundred volts to prevent entry of electrons into the extraction system from outside the thruster. Charge-exchange ions formed within the beam-extraction system and outside the thruster fall through all or a part of this potential difference, causing sputter erosion of accel surfaces and the walls of the extraction apertures. In conventional ion propulsion, accel erosion can be reduced but not eliminated by the use of a outer decel electrode, which partially shields charge-exchange ions from the E-fields associated with the accel electrode. Accel sputtering is a life-limiting process which, so far, has only been partially eliminated. In ionized-cluster thrusters, we expect that accel erosion may be an even more serious problem than it is in ion thrusters, because of the presence of the very large amount of carrier gas. This large amount of carrier gas will lead to large charge-exchange currents, but the rate of sputtering will also be reduced somewhat because the carrier-gas ions (H_2 or He) are light and have low sputtering yields.

It is also possible that the wide spread in charge-to-mass ratios present in the cluster beam may associate with a large spread in initial cluster velocities. If true, this could require the use of larger decel apertures to accommodate the varying particle trajectories; larger decel apertures would exacerbate the problem of accel erosion by allowing accel fields to penetrate into the charge-exchange plasma downstream of the decel grid. Only when further work has been done will we be able to determine the magnitude of this problem and design appropriate means to control it.

Type-3 sputtering, or direct interception on the accel grid by clusters with the energy imparted by the total screen-to-accel voltage is caused by two processes: the first results from the fact that clusters entering the extraction system have differing energies, masses, and entry points into the extraction system. The second results from the fact that the detailed shape of the electric fields near the entry point to the extraction system are subject to fluctuations induced by collective plasma effects. This means that even if all possible cluster trajectories will traverse the extraction system without impact during quiescent operation, plasma fluctuations may lead to new trajectories that will impact the grids. This sputtering process would likely be no more of a problem than it is in conventional ion thrusters, except for the perturbing effects of the retarding grid on initial cluster trajectories. The next few paragraphs, which identify a maximum specific impulse that can be achieved if we are absolutely to hold cluster energy below the sputter threshold, should be viewed as speculative, since no such limitation is needed in conventional ion thrusters.

In conventional ion thrusters, both of these types of sputtering can be controlled or eliminated by adjusting extraction-system design parameters and potentials within the discharge plasma. With a cluster beam, however, the wide range of initial cluster velocities may present difficulties in employing the conventional technology. In our studies we have not yet addressed these extraction-system design issues, but we do have a simple approach to eliminating the direct-interception: limit the cluster energies such that individual members of the cluster have energies below the sputtering threshold.

The problem of sputtering of extraction grids by clusters has been investigated previously,⁵ with the finding that sputtering does not appear to occur if the energy W_a of an individual atom within the cluster (viz., the kinetic energy that it would have if it had the same mass and velocity, but were not a part of a cluster) is below the sputter threshold for bombardment of the specific grid material by the cluster atom. That is, if, for example, 30-eV-per-atom xenon atoms or ions will not sputter molybdenum, then reference (5) suggests that neither will any number of them when they are packed together into a cluster. Since the atomic energy W_a can be written as

$$W_a = \frac{m}{2R} \left(\frac{gI_{sp}}{\eta_T} \right)^2 \quad (2.3-2)$$

the sputter threshold $W_a|_{\text{thresh}}$ sets a limit on achievable sputter-free specific impulse, independent of the size of the clusters themselves. For xenon, the sputter threshold $W_a|_{\text{thresh}}$ on molybdenum is about 35 eV, leading to a maximum specific impulse $I_{sp}|_{\text{max}}$ without sputtering of 584 s (where we have somewhat arbitrarily taken $\eta_T=1$ as a total efficiency and $R=V_B/V_T=0.8$ as an upper bound on the net-to-total voltage ratio). This is the *maximum achievable* sputter-free specific impulse, which may yet be degraded by factors such as beam divergence, nonuniform mass/charge, etc.

Equation 2.3-2 can be multiplied by the number of atoms in a cluster, n , to yield

$$W_d = \frac{M_{cl} \left(\frac{I_{sp} g}{\eta_T} \right)^2}{2R}, \quad (2.3-3)$$

where $m = M_{cl}$ is the total cluster mass. Figure 4 shows cluster-atom energy given atomic mass and maximum specific impulse. By choosing a sputtering threshold voltage and a value of specific impulse, one can estimate the range of atomic masses that can be used without risking sputter damage to the extraction system.

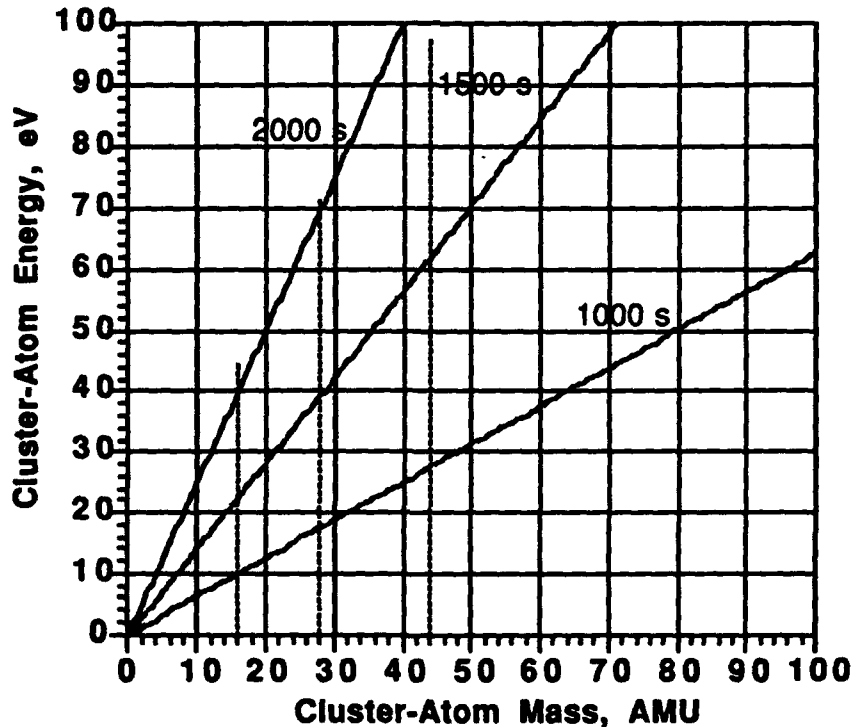


Figure 4. Kinetic energies of atoms or molecules in clusters as a function of the atomic mass number for different specific-impulse values. To avoid sputtering of the accel electrode, the energy per atom should remain below the sputter threshold (typically 25 to 35 eV), and the atomic mass number should be limited accordingly. The vertical dotted lines correspond (in increasing mass) to the masses of methane, ethylene, argon, and carbon dioxide, respectively.

2.3.2 Relationship Between Cluster Mass and Beam Voltage

Equation 2.3-3 can be rewritten in terms of the beam voltage V_B :

$$V_B = \frac{M_{cl} (I_{sp} g)^2}{2q} \quad (2.3-4)$$

Equation 2.3-4 reveals that for a given specific impulse, the beam voltage V_B is proportional to the cluster mass. Figure 5 illustrates this relationship, and shows the effect of making an arbitrary choice of upper bound of desired beam voltages. While very high voltages can certainly be accommodated in space, questions of power-supply efficiency, weight, and difficulty of insulation become significant as higher beam voltages are used.

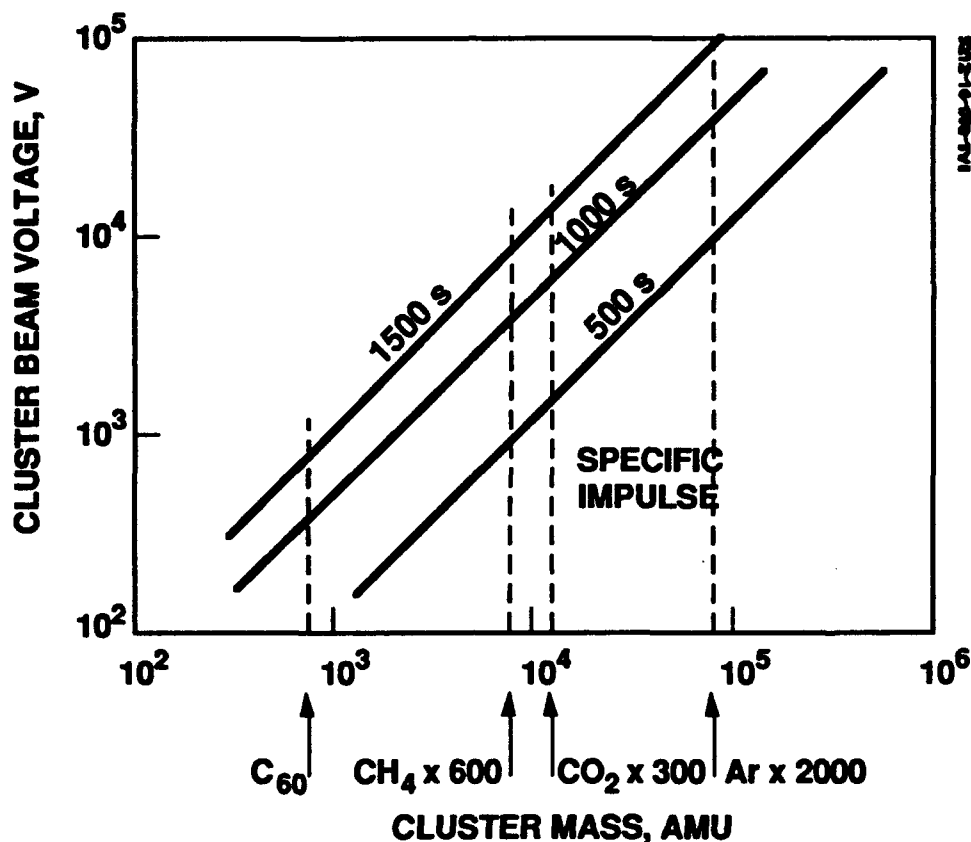


Figure 5. Cluster-beam voltage as a function of cluster mass for various values of specific impulse. A particular (arbitrary) choice for the upper bound of reasonable beam voltages is shown to illustrate the effect on choosing an appropriate cluster mass.

2.3.3 Effects of Cluster/Carrier-Gas Collisions

The flow of gas that expands from the supersonic nozzle contains clusters, carrier gas, and unclustered thrust-gas atoms. Conceivably, these collisions could destroy clusters, alter their momentum distribution, and cause other effects that could affect both the quality and current of the extracted cluster beam. In this section we briefly discuss these processes, and we conclude that the principal process of concern is that of momentum-changing collisions *within the beam-extraction system*. We do not at present know the extent to which these effects would act in an operational thruster, and additional analytical study is clearly needed.

In a previous study¹ we found that atom-cluster collisions are almost completely elastic in character, and we showed that the energy $W(z)$ of clusters varies with axial coordinate z as

$$W(z) = W_0 e^{-\frac{z}{z_0}}, \quad (2.3-5)$$

where W_0 is the initial value of the energy. We also showed that the e-folding distance z_0 is given by

$$z_0 = \frac{2m}{\left(\frac{36\rho}{mn}\right)^{1/3} V_a^{2/3} \rho}, \quad (2.3-6)$$

where ρ is the mass density of the gas of mean atomic mass m , and V_a is the volume of an atom (or molecule) of thrust gas. In evaluating equation 2.3-6 numerically, we find that the losses in energy can be very substantial: for example, a cluster composed of 300 CO_2 molecules, passing through a cloud of carrier gas having a (typical) number density of $5 \times 10^{20} \text{ m}^{-3}$ will fall to $1/e$ of its initial energy in just 40 mm. This energy is converted into increased temperature of the carrier-gas cloud, leading to a higher rate of carrier-gas atoms returning to collide with the external side of the decel electrode and the downstream side of the accel grid. While these collisions will not affect thrust, they will certainly increase the rate of charge-exchange erosion of the accel grid over the value that would obtain without the cluster collisions. The importance of this effect on accel erosion must be investigated in future work.

3.0 EXPERIMENTAL STUDY

In this section we describe the apparatus that we used in our investigation, and we present the experimental results.

3.1 TEST CONFIGURATION

Figure 1 was shown earlier to illustrate the basic arrangement of the experimental apparatus; the figure is repeated here for the convenience of the reader. The basic system consists of a plenum, into which thrust and carrier are premixed; a fast electromagnetic valve; a supersonic nozzle; an ionizer; the beam-extraction system, and a retarding-potential analyzer (RPA) that is the primary beam diagnostic. The apparatus is basically the same as in Reference (1), except that we have enlarged the ionizer to accommodate the entire beam, and we have mounted the RPA on a movable arm to facilitate probing the entire beam.

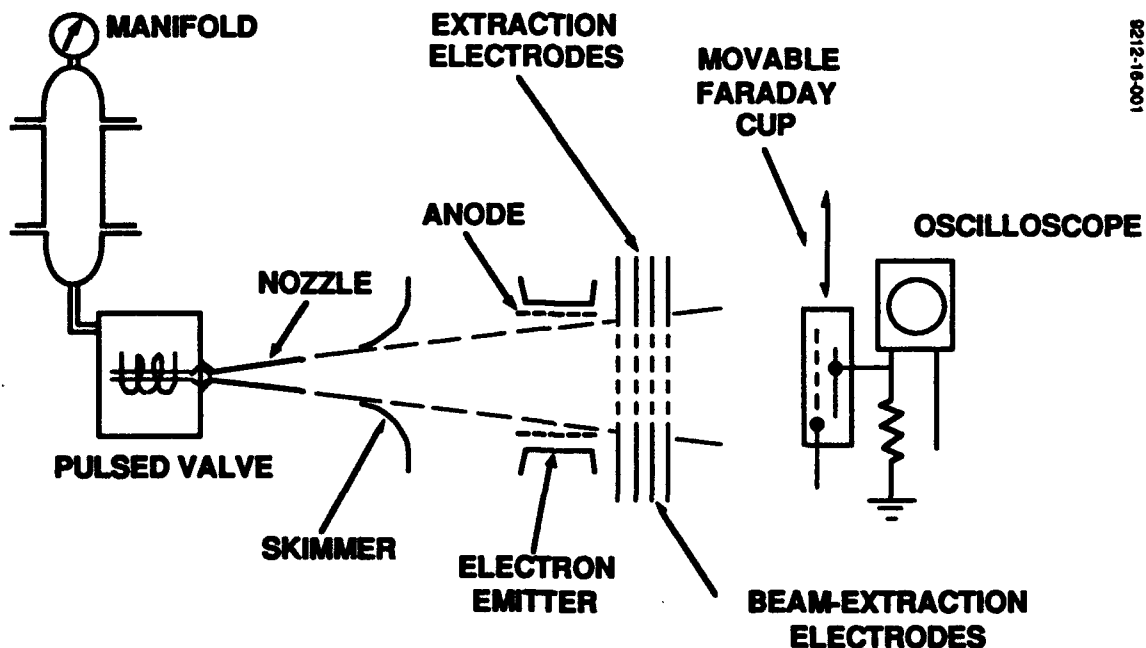


Figure 1, Duplicated from earlier in the report.

3.1.1 Pulsed Valve

In application as an ionized-cluster thruster, continuous-flow operation would be desired to provide maximum thrust and to minimize any losses that may occur during the

start-up transients. However, continuous operation produces a gas flow rate of around 30,000 liters/s at a pressure of 100 mPa. In space this and larger flow rates would pose no special problems, but in a ground test chamber it would require a very large pumping system. To avoid these difficulties we have chosen to operate our system in a pulsed mode, in which the electromagnetic valve is pulsed open for only a few ms (typically 0.5 to 2.0 ms). Our pulsed valve, which is similar to one developed by Hagen⁶ is capable of opening in as short a time as 10 μ s. We determined in our previous study¹ that the gas-flow conditions approach their steady-state values very early in a gas pulse.

3.1.2 Supersonic Nozzle

The supersonic nozzle that we have used has a minimum opening of 125 μ m and a cone angle of 8.5 degrees. The cone is 25-mm long. We found during testing that the skimmer shown in Fig. 1 had little or no effect, and most of our experimental results were obtained without it.

3.1.3 Ionizer

The ionizer consists of an anode consisting of a short cylindrical section of wire mesh (16-mm diameter, 100 mm downstream of the nozzle—an angle of about 9 degrees, to accept the entire 8.5-degree-wide beam), outside of which is the cathode, a hoop-shaped filament which provides electrons thermionically. No magnetic field is used.

In typical operation, we applied between 40 and 120 V between anode and cathode, obtaining discharge currents of between 50 and 130 mA.

3.1.4 Beam-Extraction System

The beam-extraction system that we have used was designed to be simple and easy to construct. It consists of four flat grids made from woven wire mesh having square openings 1 mm on a side. The grids each have a transparency of about 75%, and they are aligned so that the apertures are all paraxial. This construction differs substantially from conventional ion-thruster practice.

3.1.5 Retarding-Potential Analyzer (RPA)

The principal instrumentation that we used to analyze the ionized cluster beam was a simple RPA, consisting of a retarding grid and a collector, with an aperture facing the beam. We used this instrument to measure the flux, mass distribution, and profile of the ionized cluster beam.

3.2 TEST PROCEDURE

The primary thrust of our experiments under this program has been to determine the potential of ionized cluster beams as a mechanism for medium-specific-impulse space propulsion. In this section we identify these parameters and describe our methods for measuring them.

3.2.1 Thruster Parameters

The key parameters for propulsion are the total power P_{in} , the thrust F , the specific impulse I_{sp} , the propellant-utilization efficiency η_m , and the electrical efficiency η_E . The thrust is just

$$F = \frac{d}{dt}(mv) = \dot{m}_o v_{cl}, \quad (3.2-1)$$

where \dot{m}_o is the output mass flowrate and v_{cl} is the cluster exhaust velocity. It can also be written in terms of the beam parameters,

$$F = I_B \sqrt{\frac{2M_{cl} V_B}{q}} \gamma, \quad (3.2-2)$$

where I_B and V_B are the beam current and voltage, respectively, M_{cl} and q are the mass and charge of the clusters, and γ is a correction factor that accounts for cosine-law thrust loss if there is any divergence of the beam.

The specific impulse I_{sp} is the total thrust-system impulse (i.e., thrust x time) divided by the weight (not mass) of the propellant. It can easily be shown to equal

$$I_{sp} = \frac{v_{cl} \eta_m \gamma}{g} = \sqrt{\frac{2q V_B}{M_{cl}}} \frac{\eta_m \gamma}{g}, \quad (3.2-3)$$

where g is the acceleration due to gravity at the Earth's surface.

The propellant utilization efficiency is just the fraction of the input propellant mass that ends up in the thrust beam,

$$\eta_m = \frac{\dot{m}_o}{\dot{m}_i} = f_T \eta_{cl} \eta_{ion} \eta_{ext} = \frac{I_B M_{cl}}{q \dot{m}_i}, \quad (3.2-4)$$

where f_T is the fraction of the total propellant mass that is thrust gas, and η_{cl} , η_{ion} , and η_{ext} are efficiencies that correspond, respectively, to the fraction of thrust-gas atoms that become clustered, the fraction of clusters that become ionized, and the fraction of ionized clusters that successfully transit the extraction system to provide thrust. The remaining parameter, electrical efficiency η_E , is just the beam power $V_B I_B$ divided by the total power P_{in} consumed by the thruster (including beam power, discharge power, nonthrusting power to the grids such as accel current, etc.; in a practical flight thrust system, the efficiency of the power processor must also be incorporated).

$$\eta_E = \frac{V_B I_B}{P_{in}} \quad (3.2-5)$$

The expressions given in this section refer to a beam that has a single species with constant charge-to-mass ratio. Appendix 2 shows that a small but significant correction reduces performance if certain types of charge-to-mass distributions are present.

3.2.2 Measurement Methodology

In order to measure the overall propellant-utilization efficiency η_m , we determined the cluster current, the cluster mass-to-charge ratio, and the corresponding flowrate of gas through the supersonic nozzle.

In measuring the cluster current, we used our RPA as a non-energy-discriminating Faraday cup. We biased the retarding grid negative (to prevent secondary-electron emission from the collector plate which would have appeared as false cluster current), effectively using the RPA as a Faraday cup, and measured the cluster-current pulse over a cross section of the ionized-cluster beam emerging from the beam-extraction system; by integrating the current density over the beam cross-section, we obtained a value for the total cluster current.

Another key parameter is the cluster mass-to-charge ratio, M_c/q . We exploited the energy-conservation relationship

$$\frac{M_d}{q} = \frac{2V_R}{v_d^2} \quad (3.2-6)$$

to measure this parameter. Here V_R is the retarding potential applied to the RPA grid which just stops a cluster of given mass-to-charge ratio. The cluster velocity v_{cl} is determined by a time-of-flight method, measuring the time to traverse the known distance from the nozzle to the grids and timing the arrival delay from valve opening to current detection in the RPA.

The propellant-utilization efficiency η_m is calculated from the output beam current and the known total input mass flowrate \dot{m}_i of propellant into the nozzle:

$$\eta_m = \left(\frac{M_d}{q} \right) \left(\frac{I_p}{\dot{m}_i} \right). \quad (3.2-7)$$

We can also determine the product of the ionization and clusterization efficiencies by measuring the total cluster current upstream of the extraction system and comparing it to the input mass flow of thrust gas:

$$\eta_d \eta_{km} = \left(\frac{M_d}{q} \right) \left(\frac{I_d}{\dot{m}_i f_T} \right) \quad (3.2-8)$$

3.3 EXPERIMENTAL RESULTS

The technical issues outlined in preceding sections show that clusterization, ionization, and beam extraction are all key processes in achieving acceptable performance in a thruster. However, clusterization efficiency and the impact of carrier gas on propellant-utilization efficiency are the issues onto which we focused our energies, because no amount of improvement in ionization and beam-extraction technologies can compensate for poor clusterization or a requirement for excessive carrier gas.

We first tested pure inert gases (Ar and Xe), then inert-gas/carrier-gas mixtures, and finally molecular-gas/carrier-gas mixtures. We found that pure inert gases cluster very poorly, inert-gas/carrier-gas mixtures are far better but still not attractive, and molecular-gas/carrier-gas mixtures show great promise. The following sections describe these results in detail.

Figure 6 illustrates the clustering efficiency of the pure inert gases argon and xenon. These data show such low clusterization efficiencies as to be useless for practical thrusting systems.

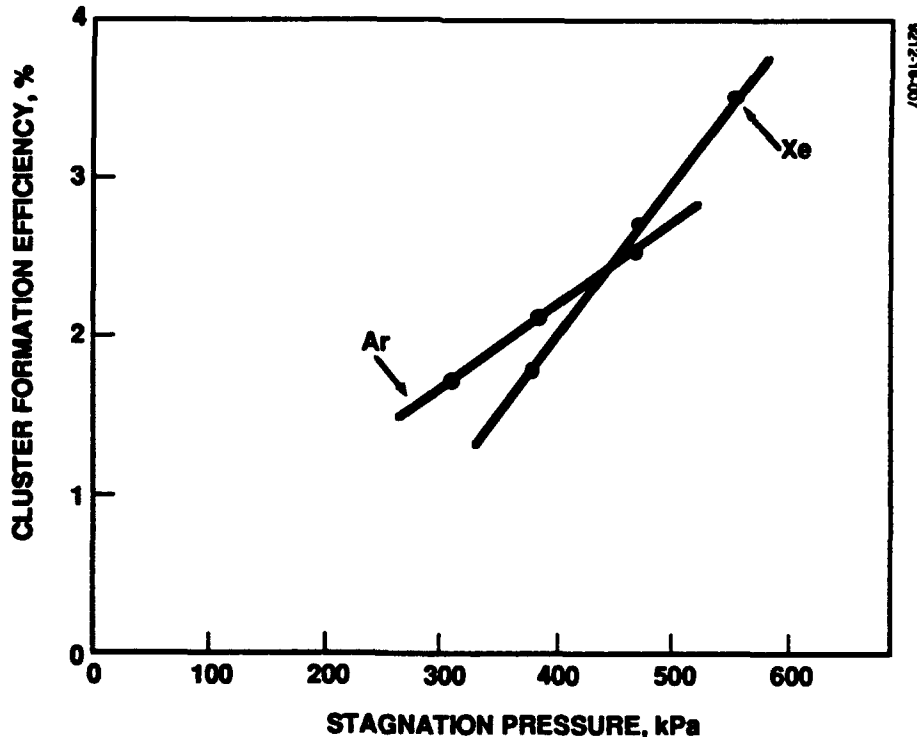


Figure 6. Clustering efficiencies (ratio of clustered gas flow to total gas flow) measured with single noble gases. The observed efficiencies are even lower than the theoretical predictions (see Figure 4), confirming that single gases are not suited for cluster thrusters.

Figures 7 and 8 show the clusterization efficiencies that we obtained with several gas mixtures, as functions of the partial pressures of the gases. In the data in Fig. 8, we have held the stagnation pressure P_0 constant at 825 kPa, while varying the partial pressures of the constituent gases: as thrust-gas partial pressure is increased, carrier-gas partial pressure is decreased to keep total pressure the same for each data point. In the upper half of the figure, hydrogen is used as the carrier gas, while helium is used for the data shown in the lower half. Remembering the arguments associated with Fig. 5, we see that the lower clusterization fractions and less desirable masses of inert-gas clusters derived either from pure gases or from thrust-gas/carrier-gas mixtures drive us in the direction of the molecular-gas/carrier-gas mixtures. Accordingly, we devoted the remainder of our experimental effort to these promising mixtures.

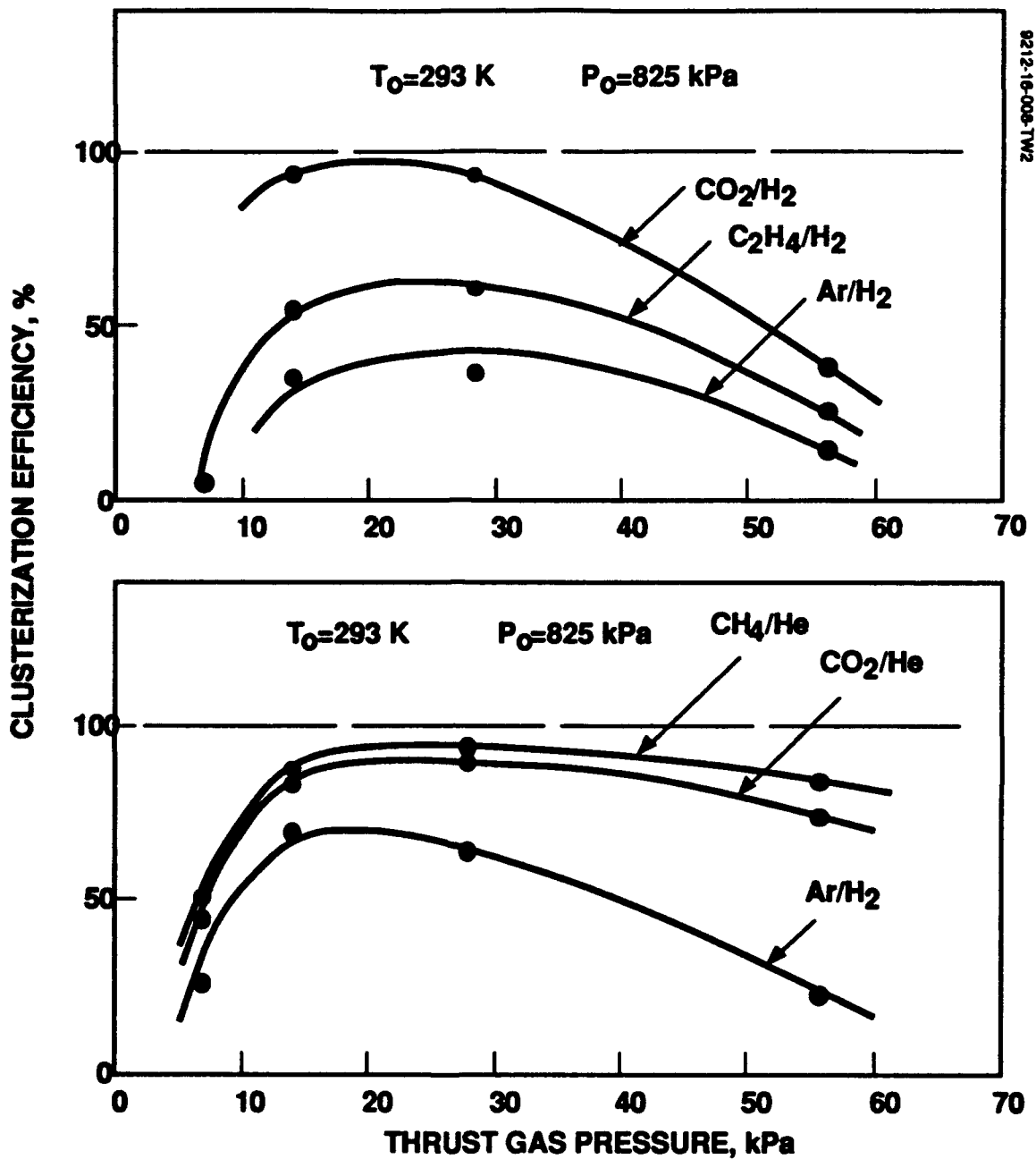


Figure 7. Clustering efficiencies measured with gas mixtures. At pressures near 27 kPa some cluster forming gases are seen to be clustered nearly completely. Accordingly, these gases are well suited for use in thrusters. However, they remain deficient in one respect: They need a larger than expected quantity of carrier gas (close to 800 kPa with 27 kPa thrust gas). This leads to a lower than predicted propellant utilization. The highest measured utilization value reached 42% .

While the data in Fig. 7 show the effect of thrust-gas partial-pressure variation of fixed total pressure, Fig. 8 illustrates the effects of variations in total pressure, with thrust-gas fraction as a

parameter. It is clear that higher total (=stagnation) pressures produce superior clusterization, except for the cases in which higher thrust-gas partial pressures are used. The best clusterization show in the figure is about 95%.

Two important results are evident in Figure 7: first, the carbon-dioxide and ethylene (C_2H_4) data show clusterization efficiencies approaching 100%, and second, there appears to be an optimum ratio of thrust gas to carrier gas at this value of the stagnation pressure. An obvious speculation that could explain this effect is that thrust-gas-atom collisions with clusters (the collisions that cause clusters to grow) are too infrequent under conditions of low thrust-gas partial pressure, and the carrier-gas fraction is insufficient to cool the growing clusters under conditions of high thrust-gas partial pressure.

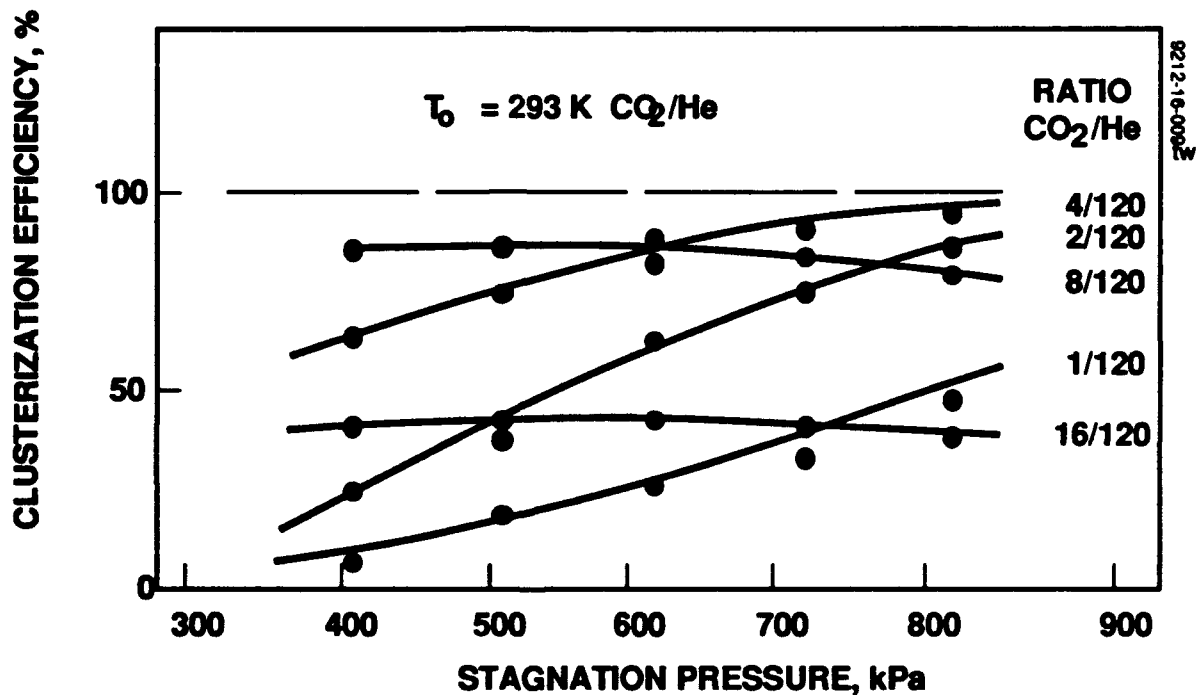


Figure 8. Dependence of clustering efficiencies on the total (stagnation) pressure, with the ratio of clustering-to-carrier gas pressures as a parameter.

From the standpoint of thruster performance, our best data were obtained with the mixture $CO_2:H_2 = 27 \text{ kPa}:800 \text{ kPa}$. Table 1 illustrates the performance calculated from the measurables identified earlier in this section. There are several important conclusions that can be reached by studying this table. The fraction of the thrust gas that actually clustered is quite high, 94%, but that fraction represents only 42% of the total mass input (the remainder being carrier gas). Also, the propellant utilization efficiency is only 15.0%, the reduction from 42% occurring in the woven-wire-mesh beam-extraction system (deduced from measurements of the ionized-cluster current on both sides of the extraction system). This low value of propellant utilization efficiency brings the specific impulse to 203 s (uncorrected for beam divergence and the presence of a distribution in q/m ; if η_m had been 100% and there were negligible beam divergence and only a single q/m species, I_{sp} would have been 1360 s). These observations point out that getting the carrier-gas flow down

substantially will be necessary before ionized-cluster beams have a chance in the space-propulsion arena. The origin of the severe current losses incurred in passing through the extraction system are unknown, but it could reside in the primitive nature of our laboratory extraction system (or possibly the presence of the retarding grid), or it may be only apparent, due to charge exchange between the cluster ions and the large amount of neutral carrier gas. This question requires further investigation.

Table 1. Ionized-Cluster Thruster Performance

Gas mixture	CO ₂ : 27 kPa, H ₂ : 800 kPa
Total mass flow	7.4x10 ⁻⁶ kg/s
Thrust mass flow	3.3x10 ⁻⁶ kg/s
Cluster Current	23.2 mA
Cluster formation and ionization efficiency	94 % (42% of total gas mass)
Propellant utilization	15.0% (after extraction)*
Average cluster size	296 molecules/e
Extracted cluster current	8.2 mA
Beam voltage	12 kV
Ionization voltage	100 V
Ionization current	100 mA
Beam power	98.4 W
Ionizer power	50 W
Electrical efficiency*	66.3% (would be 90.8 % without filament)
Thrust	14.8 mN
Thrust/Power ratio	99.8 mN/kW
Specific impulse/ γ	203 s*

* illustrates severe extraction-system losses

3.4 SUPPORTING MEASUREMENTS

In this section we describe a number of investigations that we carried out to better define our measurements of nozzle-exhaust characteristics, the cluster-ionization process, and the cluster beam.

3.2.1 Nozzle Characteristics

In Fig. 9(a), we show the velocity of pure gases expanding through the supersonic nozzle, as determined by a time-of-flight method. We believe that the decrease in velocity at low stagnation pressures may be due to boundary-layer effects. At higher stagnation pressures, the flow velocities approach their theoretical values, based on the theory of isentropic expansion into vacuum. In Fig. 9(b), however, we see a more complex shape (inset) of gas pressure arriving at the detector. We believe that the three portions of the arriving pulse correspond to carrier gas, uncondensed thrust gas, and finally, clusters. We cannot tell from these data whether the three-velocity characteristic continues, or is associated only with the leading edge of the pulse.

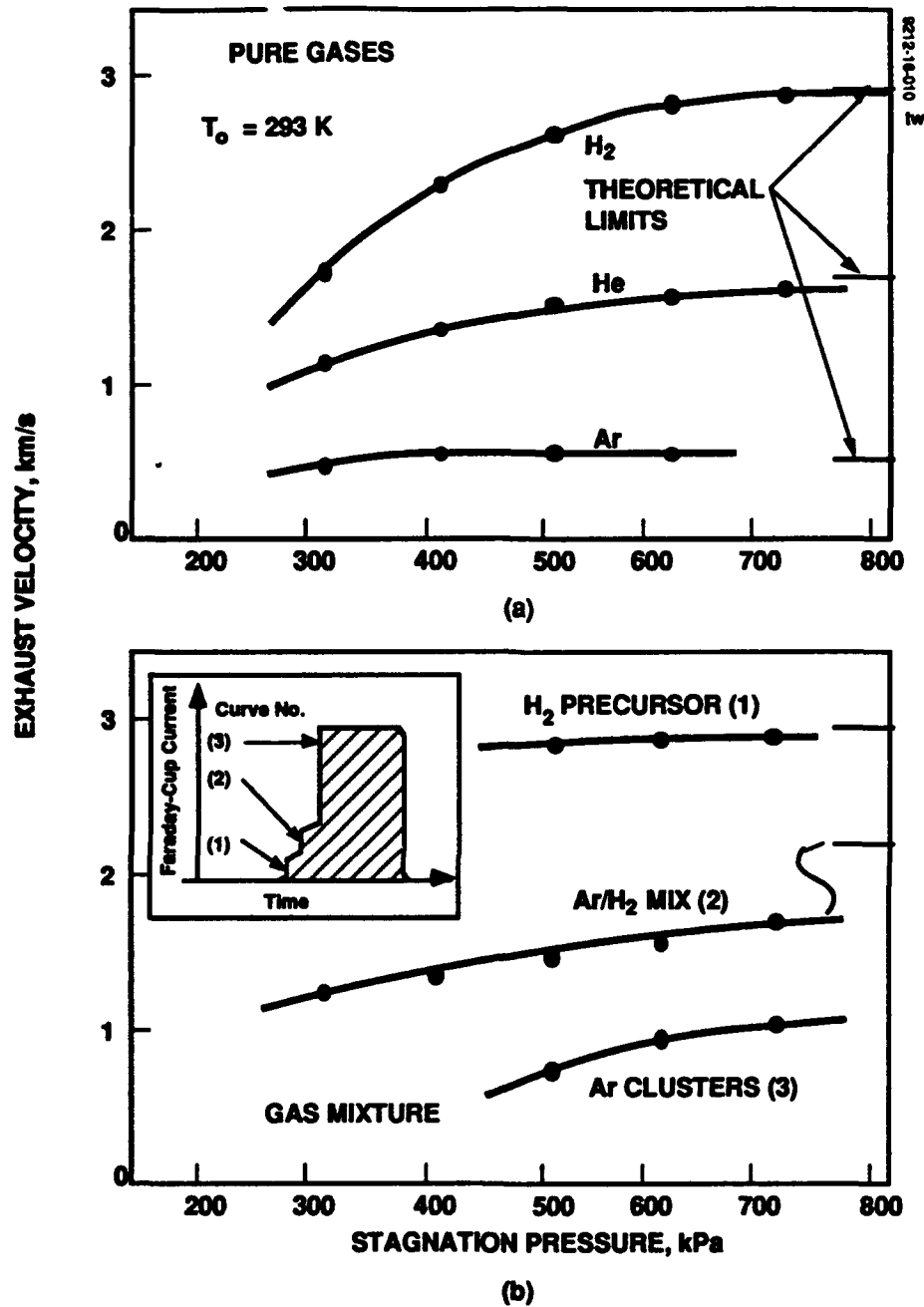


Figure 9. Exhaust velocities of single gases (top) and of a gas mixture (bottom), derived from leading-pulse-edge time-of-flight measurements. In the gas mixture with its high cluster content three different velocity groups can be distinguished: fast H₂, a slower mixture of Ar and H₂, and still slower Ar clusters. It is uncertain whether these velocities are just leading-edge effects or are steady-state phenomena.

In Fig. 10, we contrast the predictions of isentropic-expansion theory with measured data of the velocity of a pure gas (helium) and an argon-helium mixture.

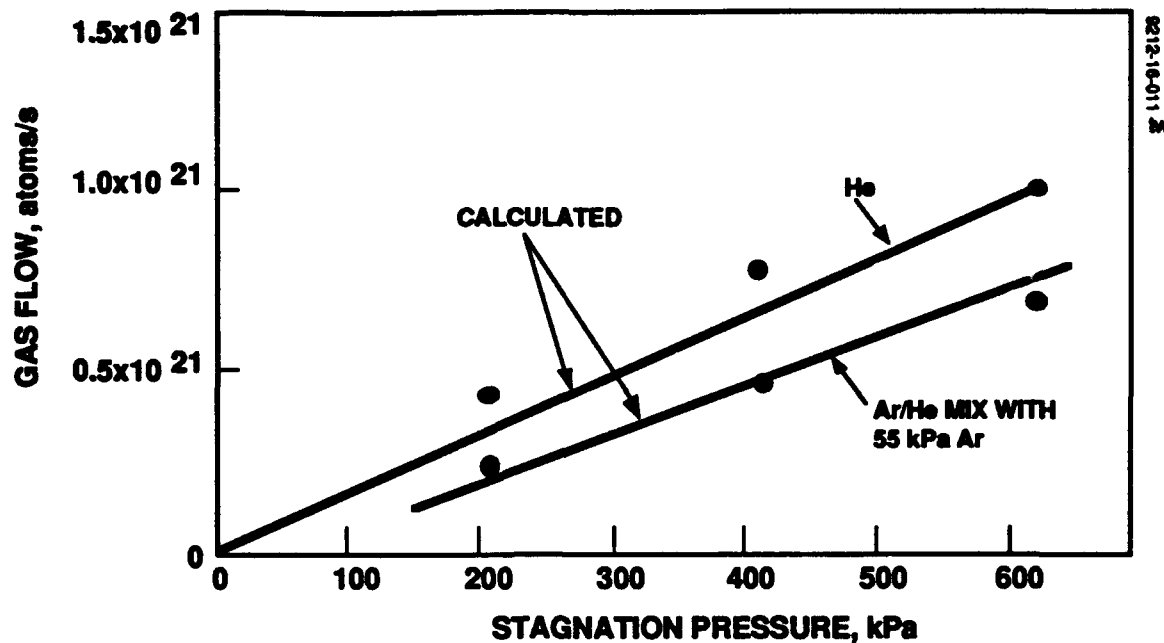


Figure 10. Calculated and measured nozzle flow rates. The calculations were based on isentropic flow conditions in the nozzle throat.

3.2.2 Ionizer Characteristics

Figure 11 illustrates the characteristics of our simple ionizer. As ionization current is increased, the cluster size is unaffected, suggesting that the ionizer does not cause cluster fragmentation; and the ionized-cluster current rises and saturates, suggesting that we are reaching either complete ionization of all clusters, or that some other saturation mechanism is coming to play.

In Fig. 12, we show the effects of varying the bias on the grid nearest the plasma (which is intended to prevent single ions from entering the beam). The sharp corner in the characteristic corresponds to the ionizer anode potential of 100 V, illustrating that the potential of the plasma near this grid resides very close to the ionizer anode potential.

As discussed in earlier sections, our simple ionizer requires excessive power in the form of filament heat, and has other characteristics that produce non-optimal performance. We feel that a hollow-cathode-based Penning-type discharge offers the best promise for averting these difficulties, but program resources did not permit us to investigate this possibility. We did, however, test a cold-cathode-based ionizer, which we found to be even less efficient than our filament ionizer.

The cold-cathode ionizer consisted of a cylindrical cone surrounding the expanding cluster beam, which was biased to between -500 V and -3000 V relative to the first (single-ion-retarding) grid of the beam-extraction system. Figure 13 compares the cold-cathode ionizer performance with that of the filament-based ionizer.

3.2.3 Beam Extraction System Characteristics

As discussed earlier, we incurred a substantial performance penalty because of the characteristics of the beam-extraction system. Late in the program, we investigated the possibility that the problem may have been that the beam was reaching space-charge limits within the extraction system. This may have been part, but is certainly not all, of the problem.

For our early data, we used grid-to-grid gaps of 6 to 8 mm in the extraction system. To determine whether these large gaps were limiting the extracted cluster currents, we reduced the spacings to 2.5 mm, and found the effects shown in Fig. 14. Since the space-charge-limited current between plane-parallel electrodes goes as the inverse of the square of the interelectrode gap, theory would predict an improvement of a factor of 6 to 8, rather than the modest factor achieved.

Figure 15 is a radial profile of the current density emanating from the beam-extraction system. The domed profile is commonly seen in ion thrusters, where the highest plasma-generation rate is near the center, but no comparable mechanism is likely to be present in our ionizer. This effect and the anomalous cluster loss through the extraction system may be due to aperture-to-aperture alignments that are inappropriate for heavy clusters.

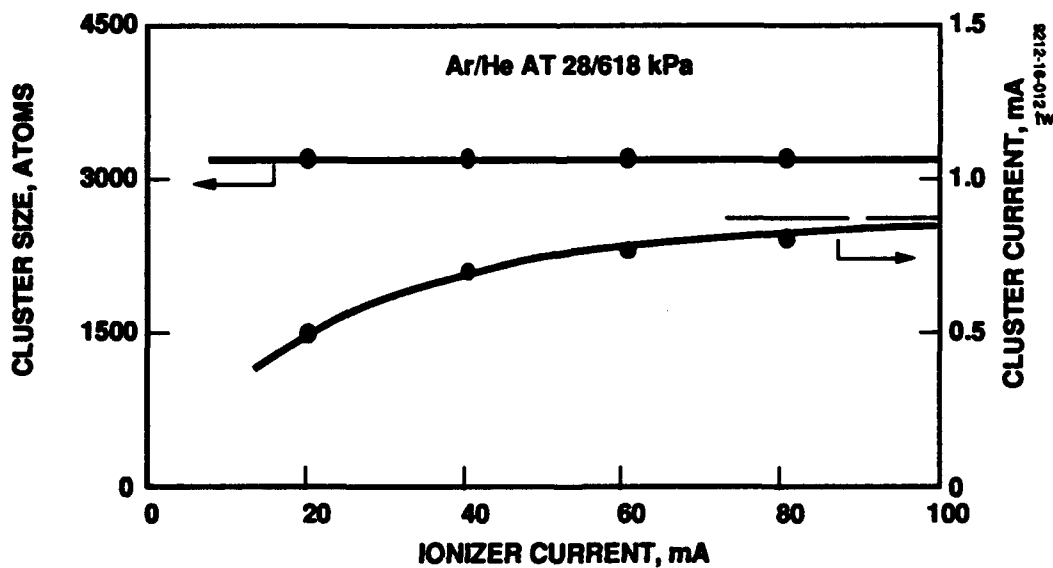


Figure 11. Cluster size and current as a function of ionizer current. The cluster current approaches a limit value which is taken to be full ionization. The independence of cluster size on ionizer current is taken as an indication that multiple ionizations do not increase with current.

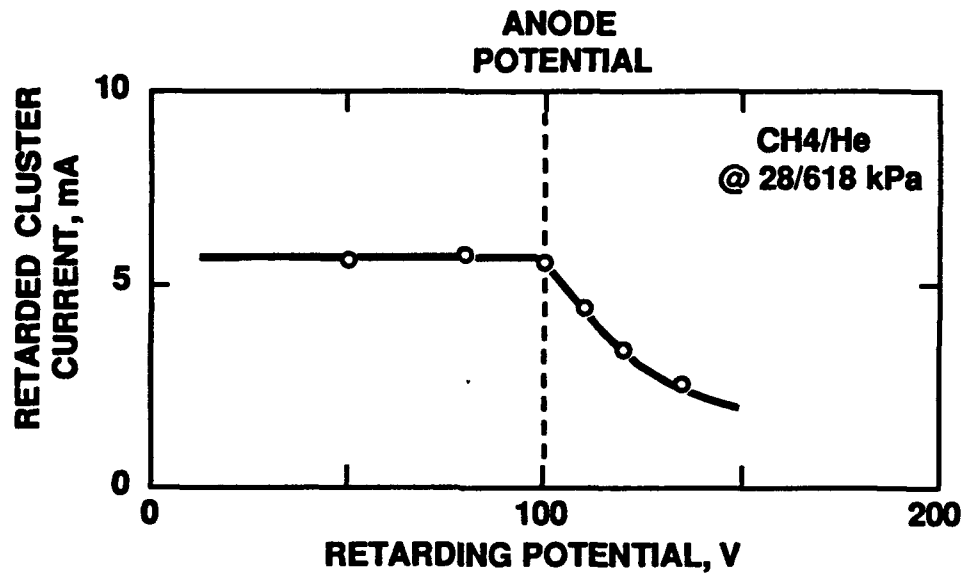


Figure 12. Retarding potential characteristic of the cluster current, measured at the retarding grid next to the ionizer. The sharp break of the curve at anode potential indicates that the potential within the ionizer is uniform, and that the plasma potential is very close to anode potential.

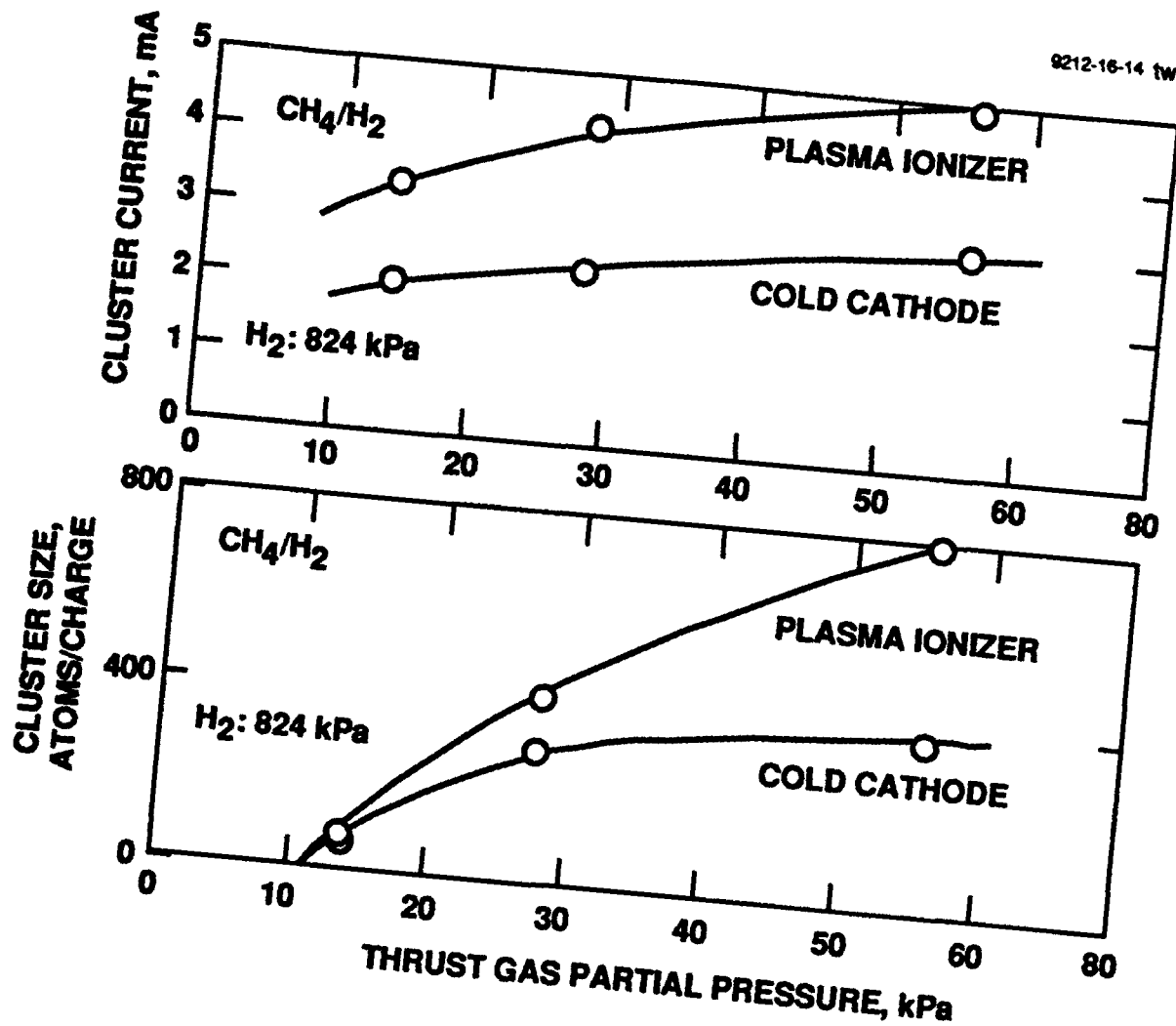


Figure 13. Comparison between plasma and cold cathode ionizers. The cold cathode ionizer clearly is less efficient. It must be added, however, that this ionizer was only briefly tested and that no attempts were made to optimize the configuration.

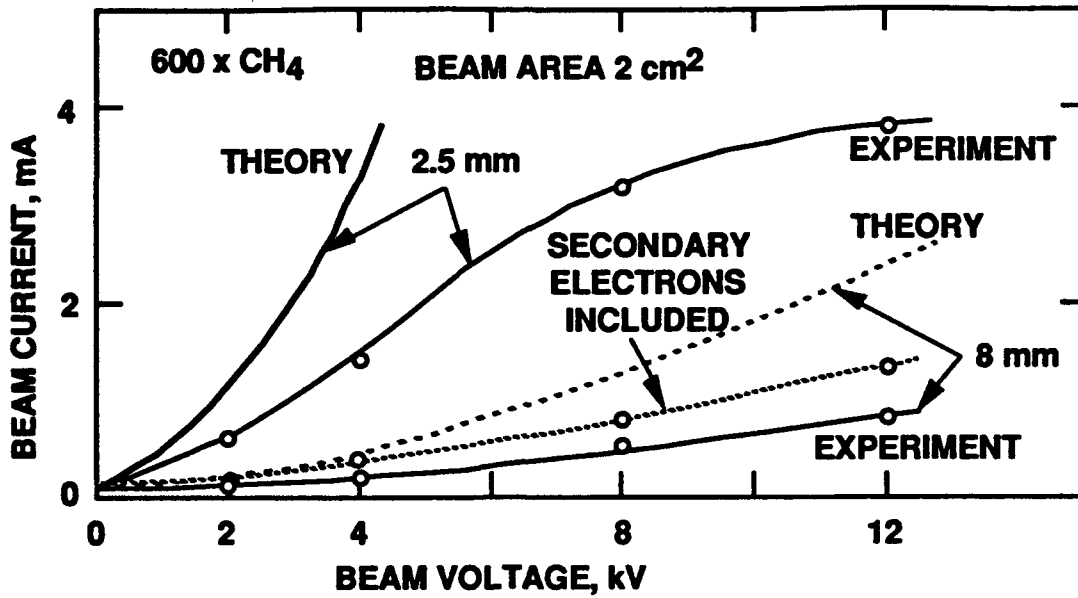


Figure 14. Observation of space-charge-limited flow in the beam-extraction system. Initially, the intergrid gap was 8 mm wide and could not, even at the highest voltages, transmit the available cluster currents. The situation improved significantly after the gap width was decreased to 2.5 mm. The dashed curve shows the substantial magnitude of secondary electron currents. These were eliminated at the Faraday cup with the help of a slightly negatively biased grid.

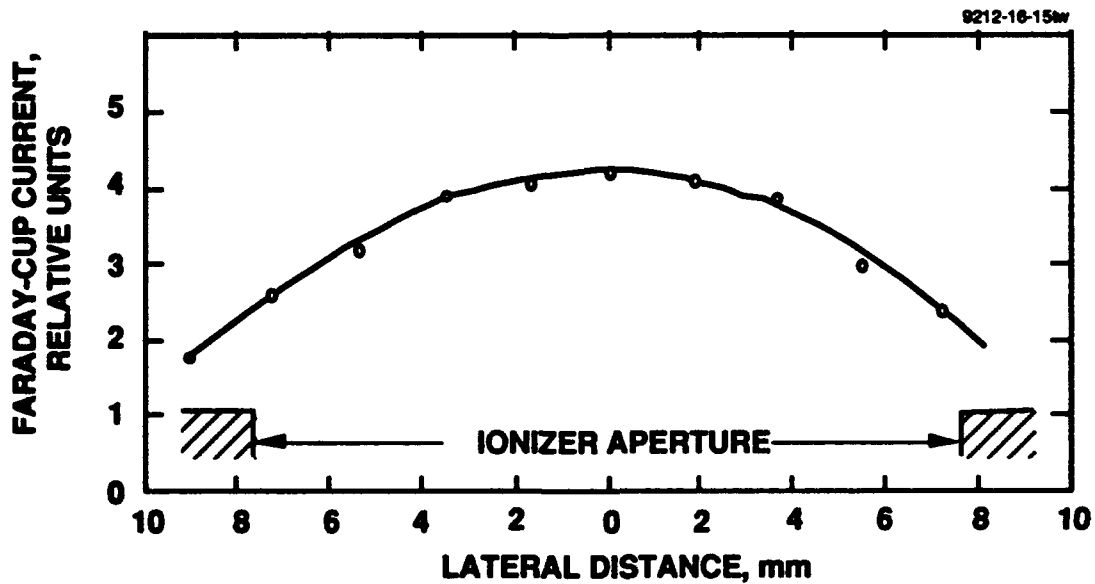


Figure 15. Transverse cluster beam distribution. Beam profiles were integrated to determine the total beam current.

4.0 SUMMARY AND CONCLUSIONS

Under this program, we have taken the first steps in demonstrating that space propulsion using ionized clusters is feasible, although a great deal of scientific and engineering work stands between our present status and having available flightready cluster-ion thrusters. We have demonstrated that we can form beams of clustered atoms or molecules, ionize them and extract them into a beam, achieving

- Thrust levels >10 mN at practical beam voltages
- Clusterization efficiencies $>90\%$ with desirable thrust gases
- Ionization efficiencies $>90\%$

Despite these accomplishments, we are presently hampered by several performance-robbing processes:

- Excessive amounts of carrier gas are needed for high clusterization, degrading mass-utilization efficiency to 40%.
- There is a substantial drop in cluster-ion current after passing through the beam-extraction system; this further degrades mass-utilization efficiency to only 15%.
- The ionizer requires excessive power (50 W), reducing electrical efficiency

We feel that these negatives are challenging but pose no clear barriers to the future development of cluster-ion propulsion to a practical reality. Without further study, we cannot with certainty foresee the path that will lead to a resolution of these issues, but we outline some ideas below that we believe worthy of investigation. Some of these ideas require scientific study, and others are simply matters of engineering that we include for completeness.

- **Carrier-Gas Injection.** The carrier gas is presently injected through the supersonic nozzle, as a mixture with the thrust gas, although the cooling benefits of the carrier gas are not needed until after the saturation point has been reached. After reviewing our present data, we believe that it may be beneficial (i.e., require less carrier gas) to introduce the carrier gas somewhat

downstream of the nozzle orifice so that it does not undergo the supersonic-flow transformation.

- **Carrier-Gas Flow Control.** Presently the drift region between the nozzle and the ionizer is completely open to the vacuum chamber, a design that is intended to avoid Paschen breakdown in the beam-extraction system. This design achieves its objective, but it may be possible to substantially enclose the drift region without incurring breakdown. This measure will inhibit the early loss of carrier gas and permit some of it to be recycled from the enclosure walls. This may be more important in a continuously operating cluster-ion thruster than it is in our pulsed device.
- **Magnetic Filter to Replace the Retarding Grid.** The retarding grid is an inefficient design for several reasons: it collects electrons from the discharge, causing an unnecessary power drain, it probably distorts trajectories of cluster ions entering the beam-extraction system, and it almost certainly interferes with the formation of the necessary meniscus-shaped plasma sheath that forms over each screen-electrode extraction aperture in beam-extraction systems that lack retarding grids. Magnetic filters, composed of strong magnetic fields transverse to the flow direction, have been demonstrated to effectively separate species with different charge-to-mass ratios, a capacity that electrostatic filters normally lack (only the velocity difference between the cluster ions and light ions allows them to be separated by electrostatic means). Such a filter could replace the retarding grid, improving the performance of the extraction system and avoiding the power drain.
- **Magnetic Confinement of the Discharge Plasma.** The discharge plasma is presently not confined at all, causing what are probably undesirably low plasma densities at the extraction system, and wasting most of the energy of the 100-V ionizing electrons. By using boundary magnetic fields to confine the plasma, these problems could be directly avoided, and the added discharge efficiency could conceivably allow operation at voltages low enough that multiply-charged clusters (with their associated performance penalty) are not formed.
- **Hollow Cathode to Replace the Filament.** This obvious measure will save a large amount of the power that is presently used to heat the filament emitter (around 3 W vs. 40 W). Hollow cathodes also have the lifetime required of flight thrusters.

5.0 REFERENCES

1. W. Knauer and R.L. Poeschel, "Cluster Beam Studies" AFOSR Final Report F49620-85-C-0125.
2. D.S. Goldin, AIAA Paper 67-85, (1967).
3. K. Oswatitsch, Z. f. Angew. Mathem. und Mech. 22, 1-14, (1942).
4. P.G. Hill, J. Fluid Mech. 25, 593-620, (1966).
5. W. Knauer, J. Appl. Phys. 67, 10-17, (1989).
6. O.F. Hagena, Z. Angew. Phys. 16, 183, (1963).

APPENDIX 1. SYMBOLS USED IN THIS REPORT

I_{sp}	Specific Impulse
M_p	Total Propellant Mass
η_T	Total Efficiency
γ	Beam-Divergence Correction Factor
g	Acceleration due to Earth's gravity
F	Thrust
P	Power
I_T	Total Mission Impulse Requirement
v	Ratio of Specific Heats
c_p	Specific Heat at Constant Pressure
c_v	Specific Heat at Constant Volume
T	Absolute Temperature
V	Volume
v_{cl}	Cluster Velocity
L	Length of ionizer cell
σ_i	Ionization Cross-Section
n	Gas Number Density
j_e	Electron Current Density In Ionizer
ϵ_0	Permittivity Of Free Space
z_0	Grid-To-Grid Gap
V_D	Discharge Voltage
m_e	Mass Of The Electron
e	Charge Of The Electron
M_{cl}	Total Cluster Mass
q	Charge
V_R	Voltage On Retarding Grid
W_a	Energy Of Atom
m	Mass Of Atom Or Ion
$I_{sp\max}$	Maximum Achievable Specific Impulse
V_B	Beam Voltage
W_{cl}	Cluster Energy
W_0	Initial Cluster Energy
ρ	Gas Mass Density
V_a	Atomic Volume
\dot{m}_0	Rate Of Output Of Mass In Thrust Beam

\dot{m}_1	Rate Of Input Of Mass To Thruster
I_B	Beam Current
η_e	Electrical Efficiency
η_{tm}	Propellant Mass-Utilization Efficiency
f_T	Mass Fraction Of Thrust Gas
η_{cl}	Efficiency Of Clustering Thrust Gas
η_{ion}	Efficiency Of Ionizing Clusters
R	Beam Voltage/Total-Extraction Voltage
N	Number Of Molecules In Cluster
P_{in}	Total Input Power To Thruster

APPENDIX 2. EFFECT OF MASS-TO-CHARGE DISTRIBUTION ON THRUSTER PERFORMANCE

As mentioned in Section 2.3, the presence of a distribution of charge-to-mass ratios q/m in the beam can cause a thruster performance loss. This loss occurs because specific impulse and the thrust-to-power ratio are related in a way that depends upon the distribution of q/m values. In this appendix we derive expressions for specific impulse and thrust-to-power ratio that are applicable to situations in which a distribution of q/m values is present, and we show the impact of the presence of the distribution.

To summarize our results, we find that the specific impulse of a beam with distributed q/m is the same that would obtain if the beam consisted of uniform q/m at the mean value of the distribution. For a given specific impulse, the thrust to power ratio is reduced by a fraction that is of order $\sigma^2/3\eta^4$, where σ is the standard deviation of the distribution, and η is its mean.

A2.1. SPECIFIC IMPULSE

Specific impulse is defined as

$$I_{sp} = F\Delta t / Mg, \quad (A2-1)$$

where F is the thrust, Δt is the duration of thrusting, g is the acceleration due to the Earth's gravity, and M is the total propellant mass. Recognizing $M/\Delta t = \dot{m} / \eta_m$, where \dot{m} is the mass flowrate in the thrust beam, and η_m is the propellant-utilization efficiency, we have

$$I_{sp} = \frac{F\eta_m}{\dot{m}g}. \quad (A2-2)$$

The thrust F is given as

$$F = \dot{m}v = \dot{m}\gamma\sqrt{\frac{2qV_a}{m}}, \quad (A2-3)$$

and we define

$$\xi \equiv \sqrt{\frac{q}{m}}, \quad (\text{A2-4})$$

giving

$$F = \dot{m} \sqrt{2V_B} \gamma \xi. \quad (\text{A2-5})$$

If, however, the mass flowrate is distributed over many ξ with a distribution function $f(\xi)$, then

$$dF = \dot{m} f(\xi) \sqrt{2V_B} \gamma \xi d\xi, \quad (\text{A2-6})$$

and, assuming γ to be independent of ξ ,

$$F = \dot{m} \sqrt{2V_B} \gamma \int_0^\infty f(\xi) \xi d\xi. \quad (\text{A2-7})$$

Finally, using A2-2,

$$I_\eta = \frac{\sqrt{2V_B} \gamma \dot{m}_m}{g} \int_0^\infty f(\xi) \xi d\xi = \frac{\sqrt{2V_B} \gamma \dot{m}_m}{g} \langle \xi \rangle. \quad (\text{A2-8})$$

In equation A2-8, note that the integral is simply the average value $\langle \xi \rangle = \left\langle \sqrt{\frac{q}{m}} \right\rangle$, so that the usual single- q/m equation holds if one substitutes an appropriately weighted average value of q/m .

A2.2 THRUST-TO-POWER RATIO

We have already obtained an expression for the thrust, eqn. A2-7, so now we need the power. In the single- q/m case, the beam power is simply $V_B I_B$, and I_B is given by

$$I_B = \dot{m} \frac{q}{m} = \dot{m} \xi^2. \quad (\text{A2-9})$$

In the case where ξ is distributed, the beam power is still $V_B I_B$; however, the beam current is now given by

$$I_B = \dot{m} \int_0^\infty \xi^2 f(\xi) d\xi. \quad (\text{A2-10})$$

Combining A2-10 and A2-7, we have

$$F/P = \gamma \eta_e \sqrt{\frac{2}{V_b}} \frac{\int_0^\infty \xi f(\xi) d\xi}{\int_0^\infty \xi^2 f(\xi) d\xi}. \quad (\text{A2-11})$$

Again notice that the numerator is the average (first moment) of the distribution $f(\xi)$, and denominator is its second moment. Equation A2-11 can therefore be rewritten more compactly,

$$F/P = \sqrt{\frac{2}{V_b}} \gamma \eta_e \frac{\langle \xi \rangle}{\langle \xi^2 \rangle}. \quad (\text{A2-12})$$

The first moment is the mean $\eta \equiv \langle \xi \rangle$, but the second $\langle \xi^2 \rangle$ moment differs from the second central moment or variance, σ^2 :

$$\sigma^2 \equiv \langle (\xi - \eta)^2 \rangle. \quad (\text{A2-13})$$

By expanding the right-hand side of Equation A2-13 and rearranging the terms, we obtain

$$\langle \xi^2 \rangle = \sigma^2 + \eta^2, \quad (\text{A2-14})$$

from which can expand the fraction $\frac{\langle \xi \rangle}{\langle \xi^2 \rangle}$ in equation A2-12 (assuming $\sigma \ll \eta$) to obtain

$$F/P = \sqrt{\frac{2}{V_b}} \gamma \eta_e \frac{1}{\eta} \left(1 - \frac{\sigma^2}{\eta^2} + \frac{\sigma^4}{\eta^4} - \dots \right). \quad (\text{A2-15})$$

The first (lowest-order) term in equation A2-15 resembles the thrust-to-power expression for a thruster involving a single charge-to-mass-ratio species; the subsequent terms give corrections when there is a spread in the charge-to mass ratios.

In this program we were unable to accurately measure the distribution of charge-to-mass ratios, so we presently have no numbers to put into equation A2-15 to estimate our performance loss. However, one thing is clear from Eqn. A2-15: if the standard deviation σ of the charge-to-mass distribution were, say, 10% of the average, η , the thrust loss due to q/m -spread will be less than 1%. This situation might arise if, for example, all clusters had the same charge and a 10% variation in mass. A potential problem arises when there are multiply-charged clusters. Suppose that the cluster beam consisted of equal parts of singly-ionized and doubly-ionized clusters having mass 250. In this hypothetical example, we find, $\eta = 6 \times 10^{-3}$ and $\sigma = 1.41 \times 10^{-3}$, in units of e/M_H , where M_H is the mass of the

hydrogen atom. The loss in thrust-to-power ratio, to third order, is then σ^2/η^2 . $\sigma^4/\eta^4 \approx 5.3 \times 10^{-2}$, or 5.3%.

For readers with ion-propulsion backgrounds, the foregoing results may seem strange, since, for example, the presence of doubly charged ions in an ion-thruster beam is normally thought to cause a substantial performance loss. The resolution of this apparent contradiction is that the analysis given in this appendix has determined the performance loss due to the fact that the *variance* of the distribution of charge-to-mass ratios in the propellant is non-zero, and effects of variation of the *mean* of the propellant mass are not discussed. In conventional ion-propulsion practice, thruster parameters are calculated with the assumption that *all* of the propellant is of a single charge-to mass ratio (e.g., Xe^+), even with the foreknowledge that other species will be present (e.g., Xe^{++}). After the fraction of Xe^{++} is determined, the performance that was calculated assuming that the beam was composed entirely of Xe^+ is corrected to reflect the true beam composition. This correction factor appears to be a performance loss (decrease in thrust-to-power, increase in specific impulse), but in fact it is simply the effect of using a propellant of higher average charge-to-mass ratio than pure Xe^+ ; it is similar to the effect of substituting Kr (a lighter gas) for Xe as a propellant, and has nothing to do with the fact that multiple species *per se* are present. (If the thruster had been assumed to operating on pure Xe^{++} instead of pure Xe^+ , then the correction factor accounting for the presence of Xe^+ would appear to be an *increase* in thrust-to-power ratio.)

Since the equations governing specific impulse and thrust-to-power ratio contain the charge-to-mass ratio only as the product qV_B/m , any change in q/m can be compensated by altering V_B to keep the product constant. A thruster with $\eta_m = \eta_E = 1$ will then exhibit identical performance with higher q/m and lower V_B . A real ion thruster may, of course, incur a change in electrical or propellant-utilization efficiency when the beam voltage is changed, so that the overall performance may indeed change as a result of the correction. This change is a different topic entirely, having to do with thruster performance curves rather than the effect of distributed charge-to-mass ratios.

**END
FILMED**

DATE:

7-92

DTIC